Construction and Building Materials 312 (2021) 125352

Contents lists available at ScienceDirect

Construction and Building Materials

journal homepage: www.elsevier.com/locate/conbuildmat

# Freeze-thaw damage evaluation and model creation for concrete exposed to freeze–thaw cycles at early-age

Dongyun Liu [a,c], Yongming Tu [a,b,c,*], Gabriel Sas [c,d], Lennart Elfgren [c]

[a] Key Laboratory of Concrete and Prestressed Concrete Structures of Ministry of Education, School of Civil Engineering, Southeast University, 211189 Nanjing, PR China
[b] National Engineering Research Center for Prestressing Technology, Southeast University, 211189 Nanjing, PR China
[c] Division of Structural and Fire Engineering, Department of Civil, Environmental and Natural Resources Engineering, Luleå University of Technology, SE-97187 Luleå, Sweden
[d] SINTEF Narvik AS, Narvik 8517, Norway

ARTICLE INFO

*Keywords:*
Early-age freeze–thaw cycles
Pre-curing time
Subsequent curing
Freeze–thaw resistance
Prediction model
Critical pre-curing strength

ABSTRACT

Concrete subjected to freeze–thaw cycles action at early-age will suffer serious physical damage, resulting in degradation of the concrete's performance. The subsequent curing conditions after early-age freeze–thaw cycles (E-FTCs) are critical to the development of the properties of frost-damaged concrete. Four test environments were set up for this study, based on different numbers of E-FTCs and subsequent curing conditions. The later-age resistance to freeze–thaw of concrete exposed to E-FTCs was evaluated by analysing the influence of pre-curing times and curing conditions. Results show that the earlier the FTCs occur, the worse the later-age freeze–thaw resistance is. In particular, for the frost-damaged concrete with a pre-curing time of 18 h, its freeze–thaw resistance is significantly worse than that of other concretes that have a longer pre-curing time. The increase in the number of E-FTCs exacerbates the damage to early-age concrete, which causes the reduced later-age freeze–thaw resistance. Subsequent water curing can significantly improve the freeze–thaw resistance of damaged concrete, while air curing is the least effective. Based on previous freeze–thaw damage models, prediction models for concrete exposed to E-FTCs were created by using the test data obtained in this study. The critical pre-curing strengths which can ensure that the damaged concrete has satisfactory frost resistance at later-age were thus obtained. For concrete structures expected to experience E-FTCs, adequate pre-curing strength and good re-curing conditions are essential.

## 1. Introduction

Freeze-thaw cycles (FTCs) action in cold environments is one of the main factors that degrade the performance of concrete structures [1]. After being subjected to FTCs, concrete can suffer severe physical damage, such as internal cracking and surface scaling. Freeze-thaw damage not only causes deterioration of mechanical properties of the concrete [2], but also increases the permeability of the concrete and the transport of external corrosive substances [3,4] e.g. chloride ions, carbon dioxide and moisture etc., which will cause corrosion of the reinforcement in concrete and pose a potential threat to the bearing capacity and safety of the whole structure.

To date, there have been comprehensive studies of the destruction mechanism of FTCs in concrete. Powers [5] first proposed the hydraulic pressure theory, and then, together with Helmuth [6], proposed the osmotic pressure hypothesis. The destruction mechanism of concrete subjected to water freeze–thaw is different to that of salt freeze–thaw. The former mainly causes internal damage to the concrete whilst the latter often leads to surface scaling [7]. It is generally believed that osmotic pressure predominantly damages concrete exposed to salt freeze–thaw. For frost damage of concrete where no external salt water is present, the destruction mechanism generally accepted is described by the hydraulic pressure theory, the micro-ice growth theory, the ice volume expansion theory and the critical degree of saturation theory [8,9]. Fagerlund [10] believed that only when the degree of saturation of concrete reaches a certain critical level can significant freeze–thaw

*Abbreviations:* DF, Durability factor; E-FTC, Early-age freeze-thaw cycle; FTC, Freeze-thaw cycle; MLR, Mass loss rate; RDME, Relative dynamic modulus of elasticity; 10-WC, Cured in water to age 28 d after 10 E-FTCs; 20-SC, Cured in standard curing room to age 28 d after 20 E-FTCs; 20-WC, Cured in water to age 28 d after 20 E-FTCs; 20-NC, Cured in natural air to age 28 d after 20 E-FTCs.

* Corresponding author at: School of Civil Engineering, Southeast University, No. 2, Southeast University Road, Jiangning District, 211189 Nanjing, PR China.
*E-mail addresses:* tuyongming@seu.edu.cn, yongming.tu@ltu.se (Y. Tu).

https://doi.org/10.1016/j.conbuildmat.2021.125352
Received 3 June 2021; Received in revised form 17 September 2021; Accepted 20 October 2021
Available online 1 November 2021

damage occur. Based on this theory, a service life prediction model of concrete in freeze–thaw environment was created [10]. After repeated FTCs, the damage to concrete is irreversible and gradually accumulative. Therefore, the process of FTCs in concrete can be regarded as being repeated fatigue loading [11,12]. Cai [13] described the freeze–thaw damage of concrete by combining the hydrostatic pressure and uniaxial tensile fatigue damage theories. Based on the classic Aas-Jakobsen fatigue life equation [14], Yu et al. [15] established the equations for determining the freeze–thaw fatigue damage in concrete subjected to water freeze–thaw and salt freeze–thaw conditions, and Tian et al. [16] proposed a prediction model for the degree of damage caused to concrete when subjected to salt freeze–thaw and flexural load combined. In addition, some classic and well-known mathematical functions or equations are often used to characterize freeze–thaw damage to concrete, such as the parabolic function [17], the Boltzmann equation [18], the inverse logistic function [19], the power function [20] and the exponential function [21].

Current studies of the frost resistance of concrete have mainly focussed on concrete materials or structures that are fully cured. In winter, or cold environments, concrete may be subjected to frost damage at an early-age stage, including freeze–thaw damage [22] and freezing damage [23]. Insufficient hydration of early-age concrete leads to a loose microstructure and low strength, so the damage by frost to concrete is very severe. Existing studies have shown that the water-cement ratio [24], the type of cement [25], the admixtures [26,27], the pre-curing time [24,28,29], the temperature [26,30] and duration [24,29] of the frost all significantly influence the performance of concrete suffering from early-age frost damage. In addition, Kong et al. [31] pointed out that, for cement-based materials subjected to early-age freeze–thaw cycles (E-FTCs), damaged fracture properties cannot be completely repaired by later-age sealed curing. By carrying out later-age positive temperature curing on early-age concrete cured at temperatures below freezing, Sang et al. [30] found that the 28-d strength of all the early frozen concrete was lower than that of control concrete continuously cured at a positive temperature. The 28-d strength of the frozen concrete deteriorated with a decrease in pre-curing time and the freezing temperature. Koh et al. [32] found that water-curing after subjected to early freezing can better improve the long-term strength of concrete than sealing-curing, and subsequent water-curing with high temperature can enhance not only long-term strength but also early strength. It follows then that the environment conditions of the later-age re-curing are a crucial factor affecting the later-age performance of early-age frozen concrete, but there have been few studies about this.

What's more, the previous prediction models of freeze–thaw damage are mainly suitable for the fully cured concrete that is not subject to frost damage, and there are no applicable damage models for early frost-damaged concrete. Creation of a prediction model for frost resistance of early frost-damaged concrete would be of great use, for example, to determine the antifreeze critical strength that is the pre-curing strength of concrete before exposed to early frost damage. At present, the antifreeze critical strength, such as specified in ACI-306R [33], depends on the mechanical properties of early frost-damaged concrete after re-curing, but does not consider its durability. Previous study shows that for early frost-damaged concrete which reached the antifreeze critical strength, by executing subsequent water-curing at 20 ℃, the 28-d strength was able to meet the requirement, but its durability was still too low [34]. Therefore, it is significant to evaluate the later-age durability of early frost-damaged concrete, e.g., freeze–thaw resistance, and then establish a corresponding degradation model to determine the antifreeze critical strength of concrete in cold environment.

In this study, a batch of concrete specimens was prepared and pre-cured for different times i.e., 18 h, 24 h, 48 h and 72 h, and then placed in a freeze–thaw environment to produce early frost damage. Subsequently, re-curing at a positive temperature was carried out on the specimens for up to 28 d. Four test environments, with different numbers of E-FTCs and re-curing conditions were set up, labelled 10-WC, 20-SC, 20-WC and 20-NC (See Section 2.3 for details). Finally, all specimens were subjected to rapid FTC tests at 28 d to evaluate the effect of the pre-curing time and the curing condition on later-age freeze–thaw resistance of concrete exposed to E-FTCs. In addition, based on the results of the freeze–thaw test and previous freeze–thaw damage models, the freeze–thaw degradation model suitable for concrete exposed to E-FTCs was created, and the critical pre-curing compressive strength required to ensure good resistance to freeze–thaw was predicted.

**Table 1**
Chemical composition, and physical and mechanical properties of Portland cement P.O 42.5.

| Chemical composition (wt. %) | | Physical and mechanical properties | |
|---|---|---|---|
| CaO | 60.82 | Specific surface area ($m^2$/kg) | 379 |
| $SiO_2$ | 20.40 | Setting time (min) | 209 (Initial setting) |
| $Al_2O_3$ | 5.20 | | 247 (Final setting) |
| $Fe_2O_3$ | 3.06 | Flexural strength (MPa) | 6.6 (3 d) |
| MgO | 1.71 | | 9.1 (28 d) |
| $SO_3$ | 3.01 | Compressive strength (MPa) | 36.5 (3 d) |
| $K_2O$ | 0.50 | | 52.5 (28 d) |
| LOI* | 2.59 | | |

* Loss on ignition.

## 2. Experimental schemes

### 2.1. Raw materials and mix proportions

Ordinary Portland cement (P.O 42.5), produced by China Cement Plant Co. Ltd, was used for this study. Its chemical composition, and physical and mechanical properties are shown in Table 1. Natural river sand with an average fineness modulus of 2.9 was used as the fine aggregate, with an average particle size of 0.35–0.5 mm; the mud concentration was less than 1.5% and the bulk density was 1410 kg/$m^3$. A secondary mixed gravel with average particle sizes of 5–10 mm and 10–20 mm with a mixing ratio of 4:6 was used as the coarse aggregate; its mud concentration was less than 0.5%, and its apparent density was 2680 kg/$m^3$. In order to ensure the good workability of fresh concrete, polycarboxylate superplasticizer SBT-801 produced by Sobute New Materials Co. Ltd was used for this study. Tap water containing no deleterious materials was used for mixing the concrete. All of the concrete samples were designed with a ratio of water to cement by mass of 0.4, as described in JGJ 55–2011 [35]. The mix proportions of the concrete are shown in Table 2.

### 2.2. Specimen preparation

Mixtures were prepared using a laboratory concrete mixer SJD-60 following standard GB/T 50080–2016 [37]. A slump test of the fresh mixture was carried out immediately after mixing; the slump value of concrete in this study was 154 mm. Subsequently, the fresh mixture was cast into plastic moulds with dimensions 100 mm × 100 mm × 100 mm for a compressive strength test and 400 mm × 100 mm × 100 mm prisms for a rapid freeze–thaw test. All concrete specimens were compacted using a vibrating table and finally cured in an indoor environment (stored at about 30 °C and above 50% relative humidity) to the planned pre-curing times i.e., 18 h, 24 h, 48 h and 72 h. All specimens were demoulded after 24 h.

### 2.3. Curing environment conditions

To evaluate the effect of early-age freeze–thaw damage on the resistance to freeze–thaw of concrete, four test environments were set up for this test. After pre-curing for different lengths of time, concrete specimens were subjected to the following curing conditions: (1) 10-WC: after 10 E-FTCs, cured in water (i.e. stored at about ~ 30–35 °C and

**Table 2**
Mix proportions of concrete.

| Mix | Mix proportions (kg/m$^3$) | | | | | Slump (mm) | 28 d $f_{cu}$* (MPa) |
|---|---|---|---|---|---|---|---|
| | Cement | Water | Sand | Gravel | Superplasticizer | | |
| OPC | 513 | 205 | 588 | 1094 | 0.30 | 154 | 52.25 |

*The cubic compressive strength value ($f_{cu}$) of concrete sample after standard curing (stored at 20 ± 2 °C and above 95% relative humidity (China GB/T 50081–2019 [36]) for 28 d.

**Table 3**
Specimen groups.

| Designation | Pre-curing time (h) | Pre-curing strength (MPa) | Curing conditions | Designation | Pre-curing time (h) | Pre-curing strength (MPa) | Curing conditions |
|---|---|---|---|---|---|---|---|
| Control | Water-curing to age 28 d after demoulding and no experiencing E-FTCs | | | | | | |
| 18–10-WC | 18 | 14.2 | 10-WC | 48–10-WC | 48 | 30.8 | 10-WC |
| 18–20-SC | | | 20-SC | 48–20-SC | | | 20-SC |
| 18–20-WC | | | 20-WC | 48–20-WC | | | 20-WC |
| 18–20-NC | | | 20-NC | 48–20-NC | | | 20-NC |
| 24–10-WC | 24 | 24.2 | 10-WC | 72–10-WC | 72 | 35.3 | 10-WC |
| 24–20-SC | | | 20-SC | 72–20-SC | | | 20-SC |
| 24–20-WC | | | 20-WC | 72–20-WC | | | 20-WC |
| 24–20-NC | | | 20-NC | 72–20-NC | | | 20-NC |

100% relative humidity) to age 28 d; (2) 20-SC: after 20 E-FTCs, cured in a standard curing room (stored at 20 ± 2 °C and above 95% relative humidity) to age 28 d; (3) 20-WC: after 20 E-FTCs, cured in water to age 28 d; (4) 20-NC: after 20 E-FTCs, cured in natural air (stored at about ~ 30–35 °C and above 70% relative humidity in laboratory) to age 28 d.

Some of the most economically active countries in the world are located in warm temperate and middle temperate regions, where the lowest temperature in winter may drop to −20 °C. So, a rapid freeze–thaw test with the temperature ranging from ~ -17 to 5 °C, lasting no more than 4 h, was carried out on concrete specimens in order to simulate the E-FTCs that occur during the winter. The freeze–thaw solution used was tap water containing no deleterious materials. To ensure the integrity of the specimen and continue to carry out subsequent tests, the number of E-FTCs should be limited. Therefore, in this test, 10 E-FTCs and 20 E-FTCs were used, which can properly damage early-age concrete specimens. In addition, one control group was set up as a reference, which was not subjected to E-FTCs and directly cured in water to 28 d after demoulding. Seventeen groups were set up and examined in this study: one control group and sixteen experimental groups, as shown in Table 3. For example, "24–20-SC" denotes concrete specimens that were subjected to 20 E-FTCs after pre-curing for 24 h, and then cured in a standard curing room to age 28 d. The results of these tests were used to examine the effects of pre-curing time, the number of E-FTCs and the re-curing conditions on the resistance to freeze–thaw of concrete.

### 2.4. Test procedures

A 2000 kN universal compression machine (WAW-2000) was used in this study, following GB/T 50081–2019 [36], to measure the values of compressive strength of each experimental group before E-FTCs (i.e., the pre-curing strength, as shown in Table 3). According to the GB/T 50107–2010 [38], due to the non-standard specimens (relative to the standard sample with dimensions 150 mm × 150 mm × 150 mm) used in this test, the measured compressive strength values of specimens needed to be multiplied by a conversion factor of 0.95. In addition, due to the strength of early-age concrete being lower than that of mature concrete, the loading rate for the compression test was set to 0.4 MPa/s [36]. The average of three specimens was used as the final value for the cubic compressive strength of each group.

The resistance to freeze–thaw of all concrete specimens, that is one control group and sixteen experimental groups, was evaluated by using a concrete rapid freeze–thaw test. NELD-FC810 concrete rapid freeze–thaw test equipment was used, and the temperature at the centre of control specimens ranged from ~ -17 to 5 °C, with each cycle lasting about 3.5 h, as shown in Fig. 1 (a) and (c). The specifications and operational steps were carried out as described in GB/T 50082–2009 [39].

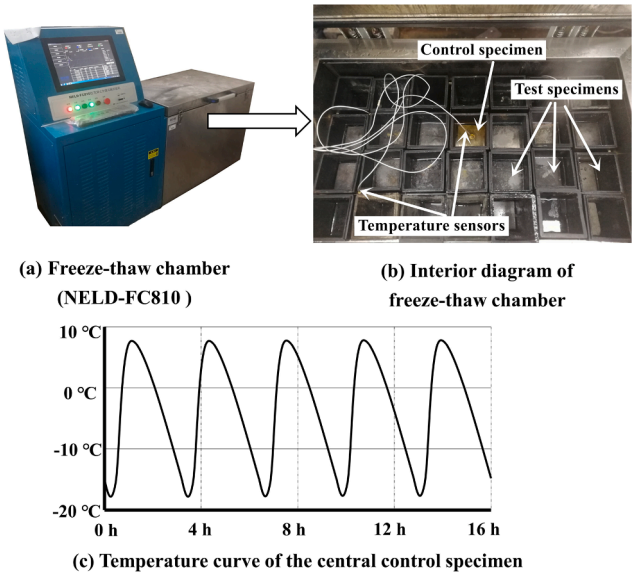


**Fig. 1.** Freeze-thaw test equipment.

The specific test steps were as follows: (i) Before the rapid freeze–thaw test, all test specimens were immersed in impurity free water for at least 4 d in order to saturate the inside of specimens. (ii) Subsequently, test specimens were taken out from the water tank, and the water on their surface was wiped clean to measure their initial mass and dynamic elastic modulus. (iii) Then, after the measurement, test specimens were placed into a freeze–thaw chamber, as shown in Fig. 1 (b). (iv) After every 25 FTCs, the mass loss rate (MLR) and relative dynamic modulus of elasticity (RDME) of test samples were measured following GB/T 50082–2009 [39], as shown in Eq. (1) and Eq. (2-2) respectively, and at the end of the test, the frost resistance durability factor (DF) (as shown in Eq. (3-1) of the concrete was calculated. Noted that the freeze–thaw process continued until the specimen had undergone 300 cycles or until its RDME had been less than 60% or until its MLR had been greater than 5%. In this study, the dynamic modulus of elasticity of each specimen was obtained by measuring its longitudinal pulse velocity using ZBL-U520 non-metal pulse velocity test equipment (as shown in

**Fig. 2.** ZBL-U520 non-metal pulse velocity test equipment.

Fig. 2). The dynamic modulus of elasticity of concrete is related to the pulse velocity of longitudinal stress waves in the concrete according to the following Eq. (2-1), as described in ASTM C597-16 [40].

$$\Delta W_n = \frac{W_0 - W_n}{W_0} \times 100\% \tag{1}$$

where $\Delta W_n$ is the MLR after $n$ FTCs (%), $W_0$ is the mass at 0 FTC (kg), and $W_n$ is the mass after $n$ FTCs (kg).

$$E = \frac{\rho V^2(1+\mu)(1-2\mu)}{(1-\mu)} \tag{2-1}$$

$$RDME = \frac{E_n}{E_0} \times 100\% \tag{2-2}$$

where $E$ is the dynamic modulus of elasticity (MPa), $\rho$ is the density of concrete (kg/m$^3$), the average density of the concrete is 2380 kg/m$^3$ in this study, $\mu$ is the dynamic Poisson's ratio, $\mu = 0.2$, $V$ is the pulse velocity of the specimen (m/s), $E_n$ is the dynamic modulus of elasticity after $n$ FTCs (MPa), and $E_0$ is the dynamic modulus of elasticity at 0 FTC (MPa).

$$DF = \frac{E_{300}}{E_0} \times 100\% \tag{3-1}$$

$$DF = \frac{0.6N}{300} \times 100\% \tag{3-2}$$

where $E_{300}$ is the dynamic modulus of elasticity after 300 FTCs (MPa). If the RDME was less than 60% or the MLR was greater than 5% before 300

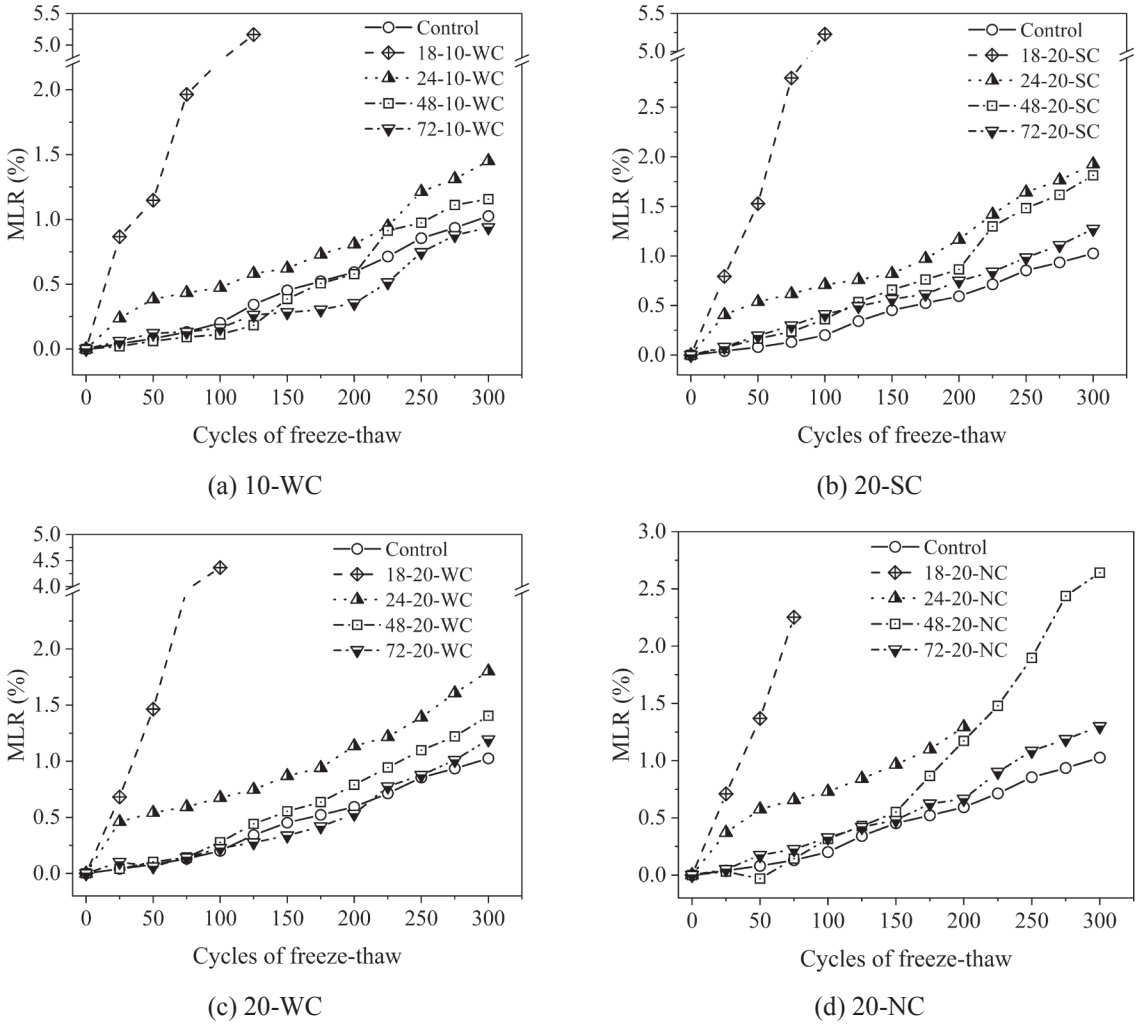


**Fig. 3.** MLRs of concrete specimens subjected to early-age freeze–thaw cycles with different curing set-ups **(a)** 10-WC **(b)** 20-SC **(c)** 20-WC and **(d)** 20-NC.

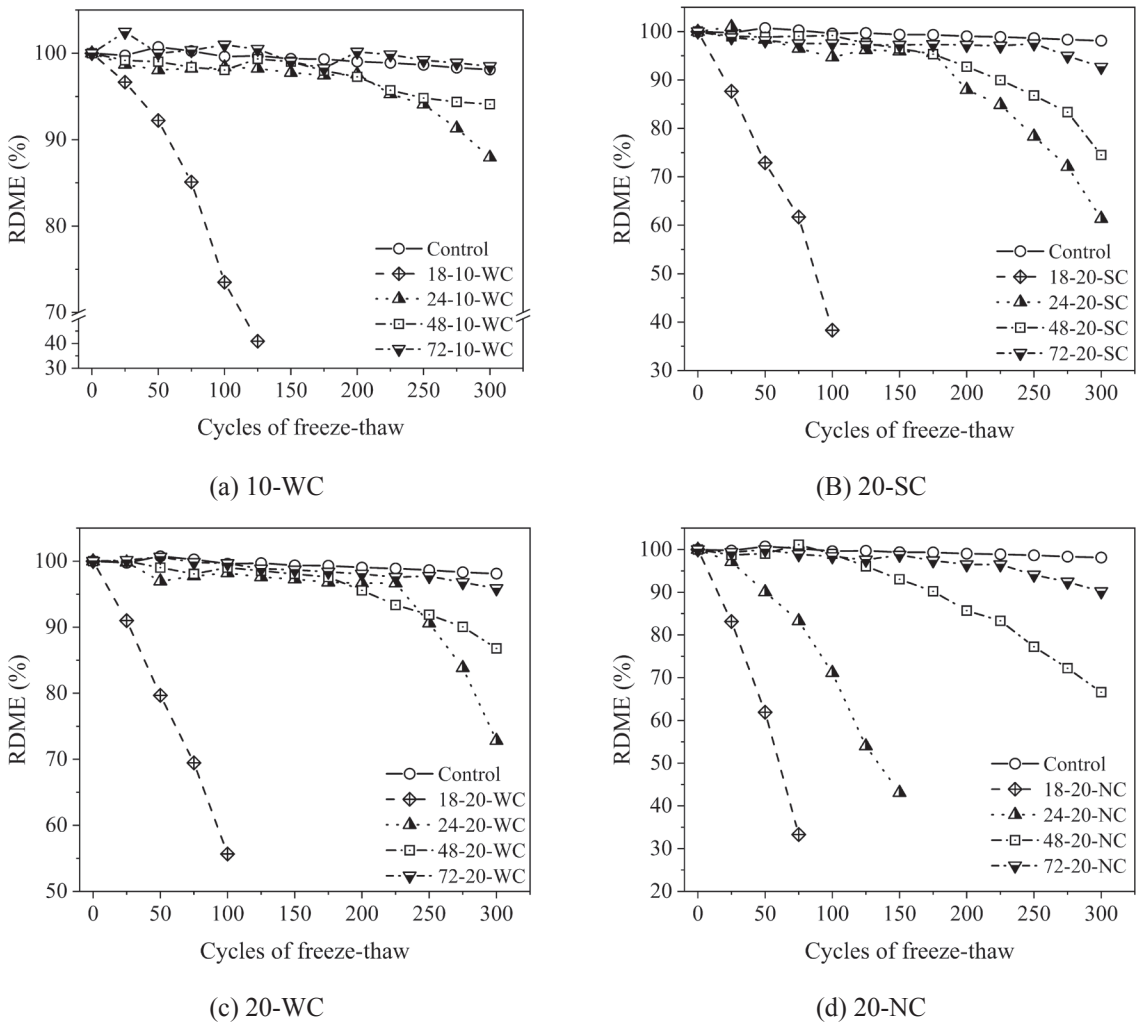


**Fig. 4.** RDMEs of concrete specimens subjected to early-age freeze–thaw cycles with different curing set-ups **(a)** 10-WC **(b)** 20-SC **(c)** 20-WC and **(d)** 20-NC.

FTCs had been applied, *DF* was calculated with Eq. (3-2) [41].

## 3. Results and discussion

### 3.1. Resistance to freeze–thaw of concrete exposed to E-FTCs

#### 3.1.1. MLR

The variations in the MLRs of the concrete specimens in the four different set-ups, plotted against the number of FTCs during the later-age freeze–thaw test, are shown in Fig. 3. As the pre-curing time increased from 18 h to 72 h, the MLRs of all the damaged concrete (i.e., concrete subjected to E-FTCs) reduced and gradually approached the value of the control specimen. The MLRs of groups 72–10-WC and 72–20-WC were slightly lower than that of the control group.

Regardless of the curing conditions, the MLRs of concrete with a pre-curing time of 18 h increased rapidly after only a few FTCs, which is different from other concrete specimens with the longer pre-curing time. For the groups 18–10-WC and 18–20-SC, their MLRs after 100 FTCs exceeded 5%, which means the specimens were deemed to have failed. It should be noted that, although the MLRs of groups 18–20-WC and 18–20-NC were smaller than 5%, the RDMEs fell below 60% before 100 FTCs, as shown in Section 3.1.2, which also means that the specimens failed.

When the pre-curing time was greater than 24 h, the MLRs of the damaged concrete significantly reduced. However, different conditions caused different change trends in the MLRs. For group 48–20-NC, its MLR started to rise after 150 FTCs and was almost 3% at 300 FTCs. Although the MLR of group 24–20-NC was within 2%, its RDME was lower than 60% at about 125 FTCs, as shown in Section 3.1.2, and the specimen was considered to have been destroyed. For the concrete specimens with a pre-curing time of 72 h, the MLR for specimens labelled "20-NC" was also higher than that for the other three curing conditions.

Therefore, the order of MLR of the damaged concrete in the four different test conditions from low to high was 10-WC, 20-WC, 20-SC and 20-NC. This indicates that the increase of the number of E-FTCs i.e., from 10 to 20, increased the MLR of concrete during the later-age freeze–thaw test. Compared with water curing and standard curing after E-FTCs, air curing with inadequate humidity decreased the resistance to freeze–thaw of the damaged concrete.

#### 3.1.2. RDME

The variations in RDMEs of the damaged concrete specimens in different test conditions, plotted against the number of FTCs during the later-age freeze–thaw test, are shown in Fig. 4. With longer pre-curing times, the RDMEs of all damaged concrete specimens increased and gradually approached, and even exceeded, that of the control group (for example, group 72–10-WC).

For the concrete specimens with a pre-curing time of 18 h, their RDMEs dropped rapidly at the beginning of the freeze–thaw test and decreased to below 60% after only 100 FTCs, indicating that these specimens can only survive for fewer than 100 FTCs. When the pre-

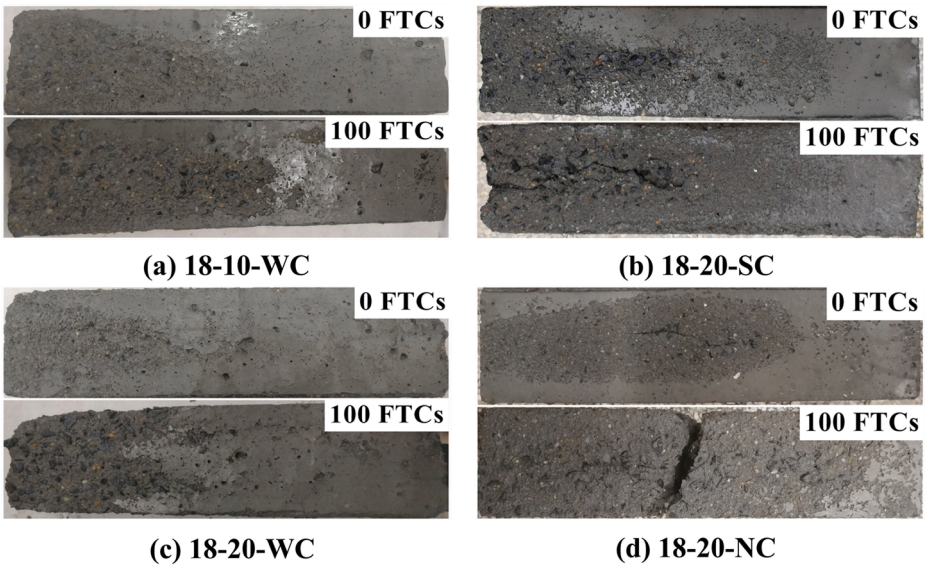


**Fig. 5.** Appearances of damaged concrete with a pre-curing time of 18 h during later-age FTCs test.

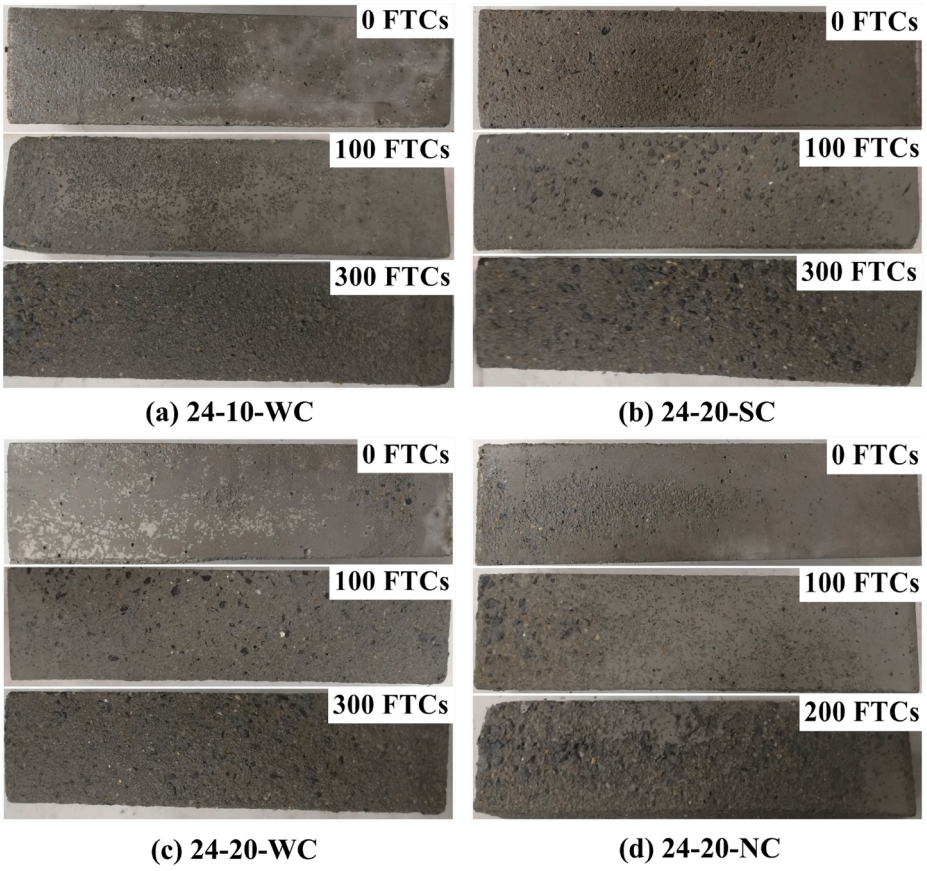


**Fig. 6.** Appearances of damaged concrete with a pre-curing time of 24 h during later-age FTCs test.

curing time was increased to 24 h or 48 h, the RDMEs of the damaged concrete specimens in test conditions 10-WC, 20-SC and 20-WC showed similar change trends, in that their RDMEs began to drop noticeably at 150–200 FTCs, but were still above 60% after 300 FTCs. However, for test condition 20-NC, the point at which the RDME decreased significantly was earlier than other test conditions. For group 24–20-NC, its RDME decreased to 54.0% after only 125 FTCs, and the specimen was deemed to have failed. The RDME of group 48–20-NC started to reduce noticeably at 125 FTCs, and reached 66.6% at 300 FTCs. For the concrete specimens with a pre-curing time of 72 h, the RDMEs for groups in the four test conditions were not much different from that of the control group, and still above 90.0% after 300 FTCs.

In general, as with the MLRs, the order of RDME of the damaged concrete in the four test conditions from high to low was 10-WC, 20-WC, 20-SC and 20-NC, which shows that the increase in the number of E-FTCs reduced the RDME of concrete during the later-age freeze–thaw

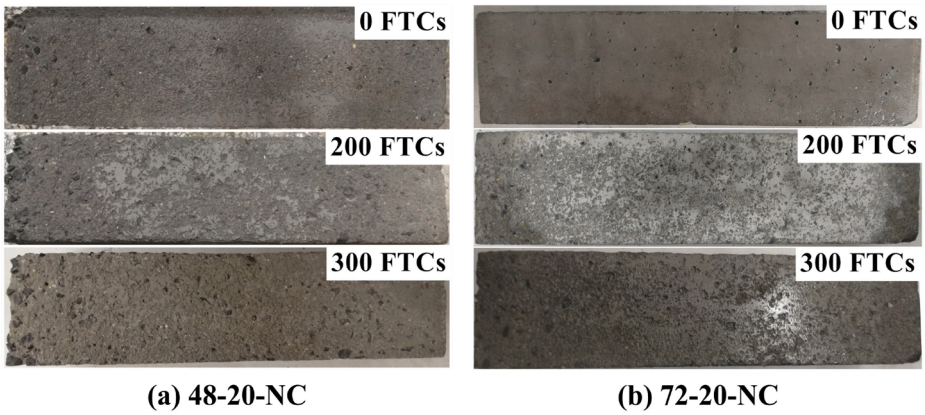


**Fig. 7.** Appearances of damaged concrete for groups 48–20-NC and 72–20-NC.

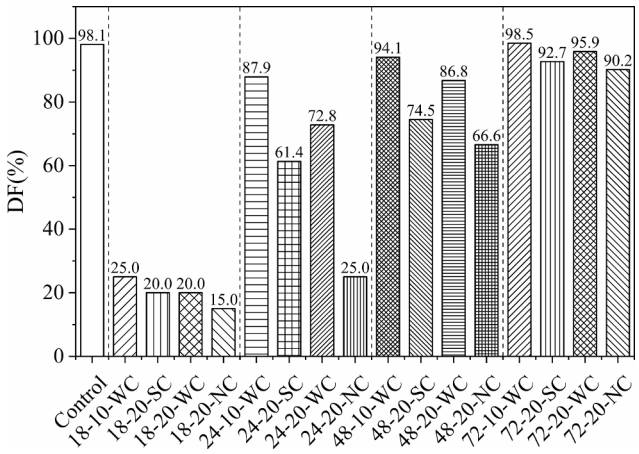


**Fig. 8.** Comparison of DFs of damaged concrete specimens.

test. Compared with water curing and standard curing after E-FTCs, air curing reduces the RDME of concrete quickest.

### 3.1.3. Appearance changes of concrete

Before and after the later-age freeze–thaw test, the changes in appearance of damaged concretes with different pre-curing times in the four different set-ups are shown in Fig. 5~Fig. 7. For the concrete specimens with a pre-curing time of 18 h (as shown in Fig. 5), there were visible damage on the specimen surface before the later-age freeze–thaw test, such as the peeling of cement pastes/aggregates, and cracks. It is

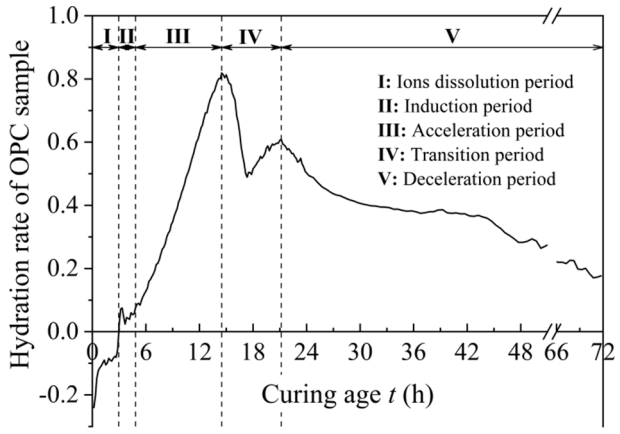


**Fig. 9.** Early-age hydration process of studied concrete OPC [43]

indicated that E-FTCs can bring more initial damage to the concrete with a pre-curing time of 18 h compared to other concretes that have a longer pre-curing time, and the damage cannot be recovered even after a long time of subsequent curing. After only 100 FTCs, these damaged concrete in the four different set-ups showed quite serious damage. For group 18–10-WC, there were few cracks but some fallen aggregates and visible pores on surface of the specimen. When the number of E-FTCs was 20, the surface of 18–20-WC group specimen had no obvious connected cracks but one end of this specimen was not in its integrity with a mass of peeling cement pastes /aggregates. Some connected cracks occurred in the surface of 18–20-SC group specimen, and even the fracture occurred in the middle of the 18–20-NC specimen.

However, when the pre-curing time was increased to 24 h, as shown in Fig. 6, there was not obvious damage on the surface of the specimen before the later-age freeze–thaw test. With the increase of FTCs, for 24–10-WC group, the damage on the surface of the specimen was mainly the peeling of cement pastes. But when the number of E-FTCs was 20, after later-age 100 FTCs, for example, visible pores and exposed coarse aggregates appeared on the surface of 24–20-SC specimen and became more as the FTCs increased.

For the specimens under the set-up "20-NC", as shown in Fig. 6 (d), Fig. 7 (a) and Fig. 7 (b), with the extension of pre-curing time, the degree of damage of the specimen surface reduced. After 200 FTCs, there were obvious cement paste peeling, aggregate loosening and matrix cracking on the surface of 24–20-NC group specimen. The surface of the 48–20-NC and 72–20-NC group specimens, after 200 FTCs, was mainly the peeling of cement pastes, and one end of the former specimen occurred some exposed and loose coarse aggregates. After 300 FTCs, the damage on the surface of the above two groups of specimens increased, but no visible cracks appeared. To sum up, with the pre-curing time prolonged, the damage degree on the surface of concrete specimens in the four different set-ups decreased, and the damage degree of specimens under the set-up "20-NC" was the highest among the four working conditions.

### 3.1.4. DF values and results analysis

Fig. 8 shows a comparison of DFs of the damaged concrete specimens subjected to different curing conditions. As pre-curing time increased, the later-age DF of concrete increased and gradually approached, and even exceeded, that of the control group (for example, 72–10-WC group). Similarly, previous studies have also showed the reduction degree of later-age various properties, e.g., strength and resistance to permeability, of early frost-damaged concrete decreases with the frost onset time prolongs [24,28]. And Hu et.al [29] pointed out the damage of the later-age performance of concrete that frozen before the final setting is obviously severer than that after the final setting. However, in this study, the DFs of the early frost-damaged concrete specimens with a pre-curing time of 18 h (after the final setting) were still significantly different from those of samples that underwent the other three pre-

curing times, and were less than a third of the control group's DF, regardless of test conditions. This is because that the frost-damage environment where the concrete exposed to was FTC action in this study but single freezing action in previous studies, and the physical damage by FTC action to concrete is more serious than that by freezing action. In addition, the resistance to freeze–thaw at early-age of concrete depends on the development of strength [42]. From the strength results from Table 3, the concrete with a pre-curing time of 18 h was only 14.2 MPa, which is significantly lower than that of other concrete with a longer pre-curing time. What's more, it is known that the strength and microstructure of concrete is relative to its hydration degree. According to the hydration results of the concrete with the same materials and mix proportion as this study [43], as shown in Fig. 9, the hydration of concrete with the age of 18 h was in a transition period from the acceleration reaction to deceleration reaction of concrete. At this stage, the internal microstructure of concrete has been basically established, but there were still some connected capillary pores. In addition, the ettringite, a main hydration product of cement, also became unstable due to the consumption of gypsum and transformed into calcium monosulfoaluminate with high density, which slows down the growth rate of the solid phase volume inside the concrete [44]. So, as Fig. 9 shows, the rate of hydration showed a temporary decrease around the age of 18 h. As the hydration continued, after 21.17 h, the hydration process of concrete was gradually dominated by diffusion reaction, and the hydration reaction of cement became stable and slow. At this period, the hydration products gradually filled the pores and the permeability channel would be transformed from the capillary pores to the gel pores, resulting in a huge reduction in permeability [45]. Previous studies showed when the permeability of concrete drops significantly is about the age of 24 h, which is called the critical age of capillary damming [46]. Therefore, for the concrete with a pre-curing time of 18 h, on the one hand, due to its low compactness and high permeability, its internal pores are susceptible to saturation during the E-FTCs; on the other hand, the low strength causes the pores easily to be destroyed by freezing expansion and hydrostatic pressure. So, after being subjected to E-FTCs, serious internal damage occurs and is not repaired completely, even after performing subsequent curing [47], resulting in poor resistance to freeze–thaw at later-age. After the age of 24 h, the permeability of concrete obviously dropped, and the damage of E-FTCs to concrete was not serious with the result that most damage would be restored and then the concrete had quite satisfactory later resistance to freeze–thaw.

Comparing the DFs of the damaged concrete specimens having undergone different pre-curing times and test conditions, the order of DFs of concrete in the four test conditions from high to low was 10-WC, 20-WC, 20-SC and 20-NC, except for groups 18–20-SC and 18–20-WC, which had the same DFs. That indicates that the greater the number of E-FTCs, the lower the DFs of the damaged concrete at later-age. And, the resistance to freeze–thaw of the damaged concrete with water curing after E-FTCs was the best, followed by standard curing, whilst natural curing was the worst. During the E-FTCs, repeated FTCs, as with fatigue loading, will cause a continuous build-up of internal damage to the concrete [11]. Therefore, the greater the number of E-FTCs, the more serious the internal damage and thus poorer durability at later-age. Although the re-curing process after E-FTCs cannot completely repair the internal damage caused by the E-FTCs to the concrete, compared with natural air curing, water curing and standard curing can provide sufficient moisture for the further hydration of the concrete, which is conducive to better development of the concrete microstructure [48,49]. In addition, compared to the standard curing, there was the higher curing temperature in subsequent water curing environment, which is also helpful to improve the hydration rate and resistance to freeze–thaw of concrete [50]. By contrast, natural air curing involves inadequate moisture, so the internal pores of the concrete will experience a self-desiccation phenomenon, which makes the local pore structure of concrete loose and the pore size increase [51,52,53,54]. These larger local pores facilitate freeze–thaw damage in specific areas during the later-age freeze–thaw test, resulting in the decrease in the resistance to freeze–thaw of the concrete. The different appearances of the damaged concrete specimens with a pre-curing time of 24 h during the later-age freeze–thaw test in three test conditions i.e., 20-SC, 20-WC and 20-NC are shown in Fig. 6 (b), Fig. 6 (c) and Fig. 6 (d). At 100 FTCs, peeling of cement mortar and aggregate appeared on the surface of the three groups of specimens. The peeling in groups 24–20-SC and 24–20-WC was uniformly distributed over the entire surface and the depth of peeling was shallow, while the severe surface peeling mainly occurred at one end of the specimen for group 24–20-NC. At 200 FTCs, the degree of peeling increased for groups 24–20-SC and 24–20-WC, and a few microcracks appeared. However, for group 24–20-NC, not only had the peeling spread all over the surface, but also the damage at the end had become very serious, with some coarse aggregate detaching and a small number of connected cracks visible. The specimen was deemed to have failed and its resistance to freeze–thaw was the worst between the three groups of specimens. Therefore, the subsequent curing conditions have a great influence on the resistance to freeze–thaw of concrete exposed to freeze–thaw cycles at early-age. To ensure that the damaged concrete has a satisfactory frost resistance at later-age, adequate subsequent wet curing should be carried out.

### 3.2. Freeze-thaw damage model of concrete exposed to E-FTCs

#### 3.2.1. Damage model of concrete based on RDME

Freeze-thaw of the concrete negatively affected mechanical properties, such as elastic modulus, compression strength, tensile strength and RDME, and increased surface peeling and mass loss of concrete [2,55,56]. Of these properties, RDME is a good indicator of the damage being caused to the concrete sample and is often used in freeze–thaw damage models because it is easy to measure non-destructively [57]. The process of freeze–thaw damage in the concrete is similar to the process of fatigue damage in concrete subjected to repeated loading and unloading. Some previous studies [13,16] have utilized the fatigue damage accumulation theory, such as Chaboche's fatigue damage model and Aas-Jakobsen's fatigue life prediction model, to characterize the freeze–thaw damage to concrete.

Pei et al. [58] proposed a model of freeze–thaw deterioration of concrete based on Chaboche's fatigue damage theory [59], as shown in Eq. (4). This equation describes the variation in RDME of concrete being subjected to a number of FTCs.

$$R_n = \frac{E_n}{E_0} = [1 - \beta_2 n(1-\beta_1)]^{\frac{1}{1-\beta_1}} (\beta_1 \neq 1) \tag{4}$$

where $\beta_1$ and $\beta_2$ are the material parameters, which are related to the freezing rate, temperature and medium of the freeze–thaw process and the material itself.

In addition, Yu et al. [15] established a damage model of freeze–thaw in concrete subjected to a water freeze–thaw environment based on the Aas-Jakobsen S-N equation [14], as shown in Eq. (5-1). It should be noted that the model suggested that the damage threshold of concrete in these conditions is 40%, following ASTM C666M-15 [60] and GB/T 50082–2009 [39].

$$R_n = \frac{E_n}{E_0} = \frac{0.6 logN}{logN - 0.4 log(N-n)} \tag{5-1}$$

$$\beta = \frac{0.4}{logN} \tag{5-2}$$

where $N$ represents the maximum number of FTCs of concrete under laboratory conditions, and $\beta$ is the material parameter.

Therefore, in this study, two types of damage model, the Pei model (Eq. (4)) and the Yu model (Eq. (5-1)), were used to describe the relationship between RDME of the early frost-damaged concrete and the number of FTCs. Then, the relationship between the material parameters

**Table 4**
Material parameters $\beta_1$ and $\beta_2$ in the Pei model and the coefficients of determination for each group.

| NO. | $\beta_1$ | $\beta_2$ (×10^-5) | $R^2$ | NO. | $\beta_1$ | $\beta_2$ (×10^-5) | $R^2$ |
|---|---|---|---|---|---|---|---|
| 18–10-WC | −4.3689 | 148.00 | 0.9985 | 48–10-WC | –22.5581 | 11.53 | 0.9553 |
| 18–20-SC | −0.8543 | 446.00 | 0.9953 | 48–20-SC | −13.0013 | 23.44 | 0.9785 |
| 18–20-WC | −0.8009 | 361.00 | 0.9993 | 48–20-WC | −20.3873 | 14.89 | 0.9656 |
| 18–20-NC | −0.7934 | 640.00 | 0.9999 | 48–20-NC | −6.1801 | 44.26 | 0.9532 |
| 24–10-WC | −16.5094 | 16.49 | 0.9366 | 72–10-WC | −50.2846 | 2.85 | 0.7466 |
| 24–20-SC | −7.6520 | 38.02 | 0.9558 | 72–20-SC | −35.6280 | 8.49 | 0.6165 |
| 24–20-WC | −15.1414 | 20.53 | 0.9297 | 72–20-WC | −48.9083 | 5.86 | 0.9749 |
| 24–20-NC | −1.7038 | 224.00 | 0.9798 | 72–20-NC | −27.3815 | 11.16 | 0.9693 |

**Table 5**
Material parameter $\beta$ in the Yu model and the coefficients of determination for each group.

| NO. | $N$ | $\beta$ | $R^2$ | NO. | $N$ | $\beta$ | $R^2$ |
|---|---|---|---|---|---|---|---|
| 18–10-WC | 125.00 | 0.1908 | 0.9651 | 48–10-WC | 682.50 | 0.1411 | 0.8578 |
| 18–20-SC | 76.13 | 0.2126 | 0.2589 | 48–20-SC | 327.68 | 0.1590 | 0.9072 |
| 18–20-WC | 100.36 | 0.1998 | 0.7160 | 48–20-WC | 454.06 | 0.1505 | 0.8626 |
| 18–20-NC | 51.27 | 0.2339 | 0.5358 | 48–20-NC | 302.91 | 0.1612 | 0.9196 |
| 24–10-WC | 508.21 | 0.1478 | 0.7890 | 72–10-WC | 2139.57 | 0.1201 | 0.2796 |
| 24–20-SC | 301.20 | 0.1614 | 0.9434 | 72–20-SC | 681.56 | 0.1412 | 0.6394 |
| 24–20-WC | 340.43 | 0.1580 | 0.7076 | 72–20-WC | 1012.86 | 0.1331 | 0.8660 |
| 24–20-NC | 150.01 | 0.1838 | 0.6267 | 72–20-NC | 557.48 | 0.1457 | 0.8503 |

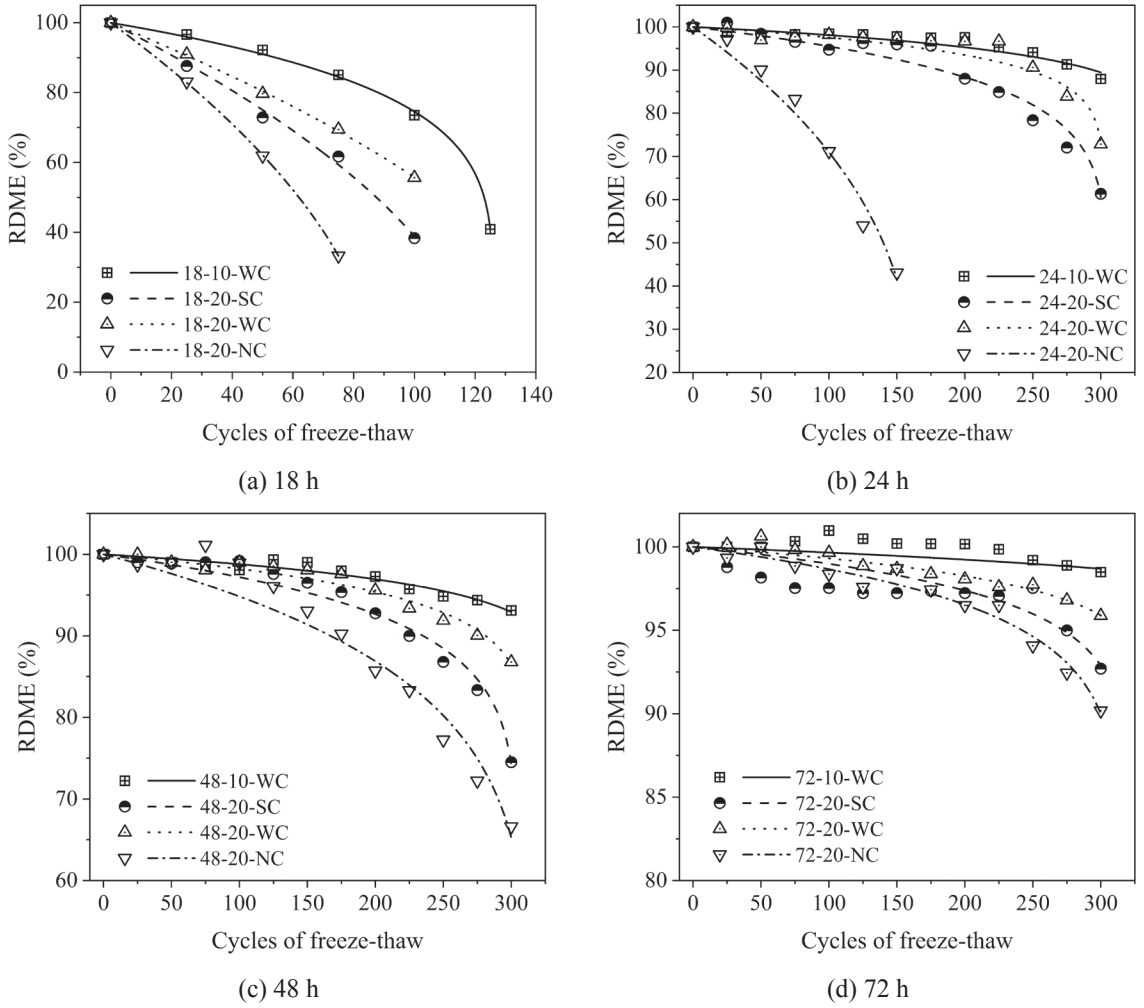


**Fig. 10.** Fitting curves of RDME and the number of FTCs using the Pei model when the pre-curing times were **(a)** 18 h **(b)** 24 h **(c)** 48 h and **(d)** 72 h.

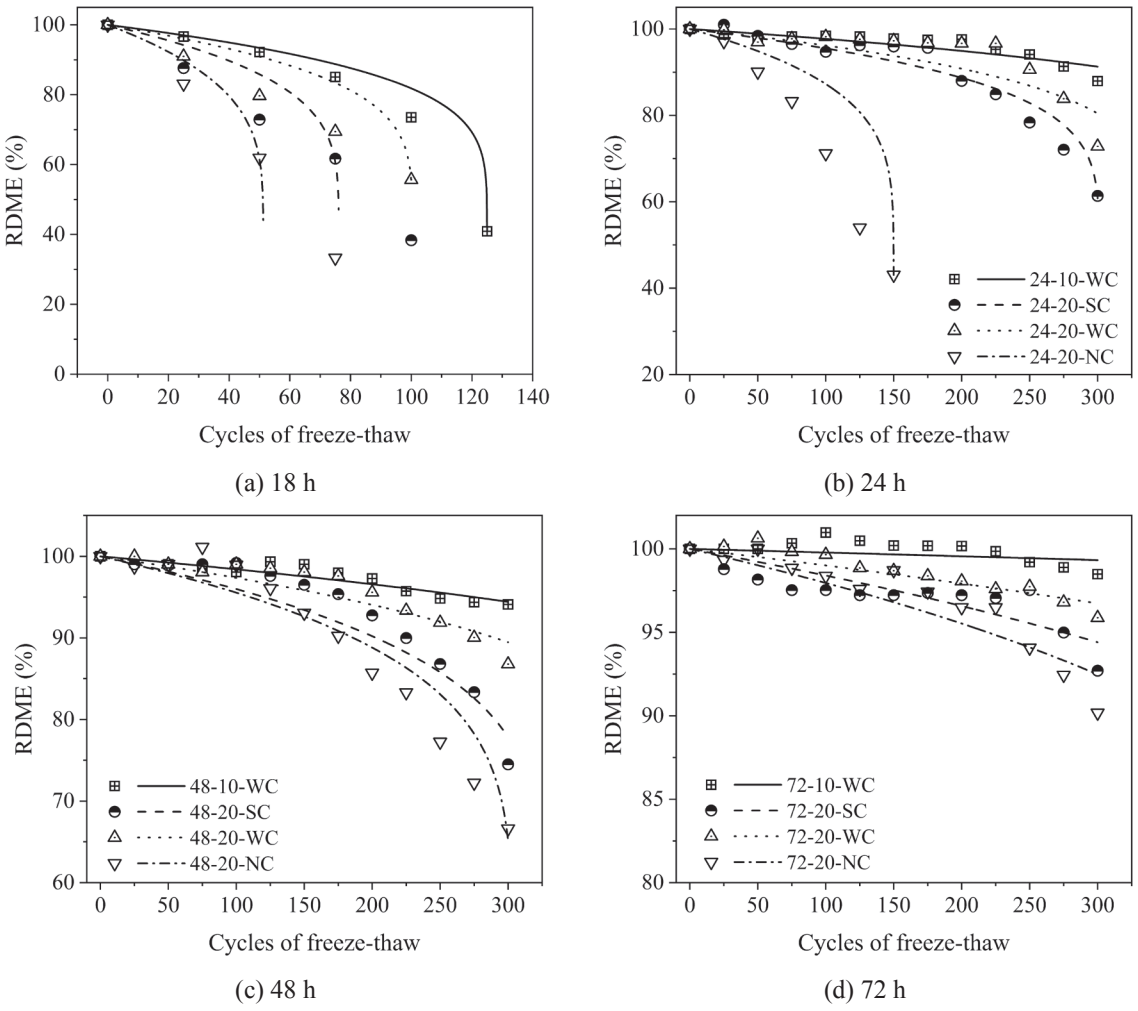


**Fig. 11.** Fitting curves of RDME and the number of FTCs using the Yu model when the pre-curing times were **(a)** 18 h **(b)** 24 h **(c)** 48 h and **(d)** 72 h.

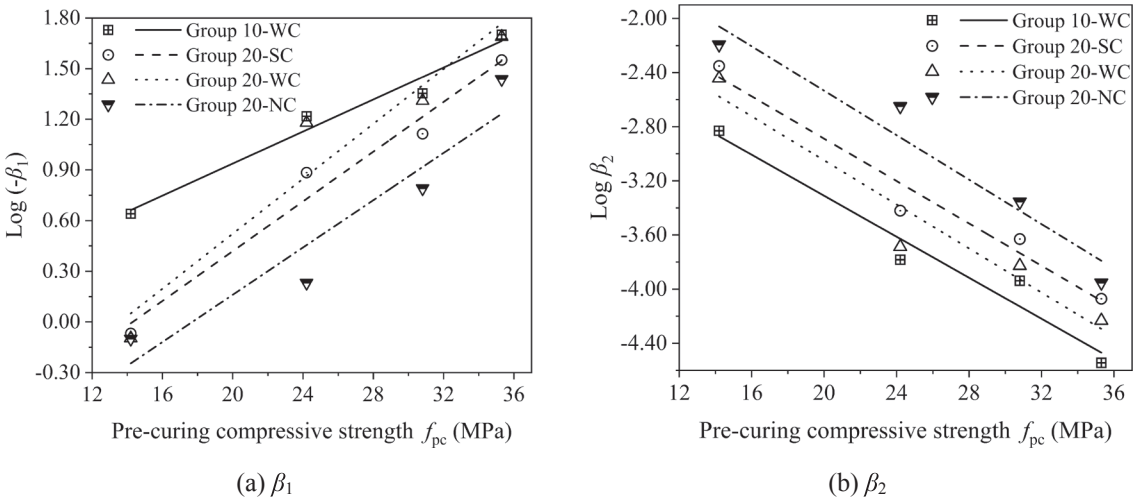


**Fig. 12.** Relationship between material parameters **(a)** $\beta_1$ and **(b)** $\beta_2$ in the Pei model and pre-curing compressive strength of the damaged concrete specimens.

in the damage models and the pre-curing strengths of concrete ($f_{pc}$) was analysed to create a freeze–thaw damage model that was suitable for early frost-damaged concrete specimens with different pre-curing strengths. Finally, the critical pre-curing strengths ($f_{pc\text{-}crit}$) that can ensure adequate later-age resistance to freeze–thaw of the damaged concrete in the four curing test conditions were obtained.

### 3.2.2. Material parameters of the freeze–thaw damage model

Based on the test results of RDME of the damaged concrete specimens in the four test conditions, the materials parameters of two types of

**Table 6**
Fitting equations for material parameters $\beta_1$ and $\beta_2$ in the Pei model with pre-curing compressive strength $f_{pc}$.

| Groups | $\beta_1$ | $R^2$ | $\beta_2$ | $R^2$ |
|---|---|---|---|---|
| 10-WC | $\beta_1 = -10^{-0.01162 + 0.04746 f_{pc}}$ | 0.9696 | $\beta_2 = 10^{-1.79538 - 0.07573 f_{pc}}$ | 0.9554 |
| 20-SC | $\beta_1 = -10^{-1.05421 + 0.07367 f_{pc}}$ | 0.9730 | $\beta_2 = 10^{-1.32452 - 0.07822 f_{pc}}$ | 0.9631 |
| 20-WC | $\beta_1 = -10^{-1.10502 + 0.08136 f_{pc}}$ | 0.9246 | $\beta_2 = 10^{-1.42187 - 0.08136 f_{pc}}$ | 0.9328 |
| 20-NC | $\beta_1 = -10^{-1.23926 + 0.07001 f_{pc}}$ | 0.9055 | $\beta_2 = 10^{-0.89298 - 0.08209 f_{pc}}$ | 0.9435 |

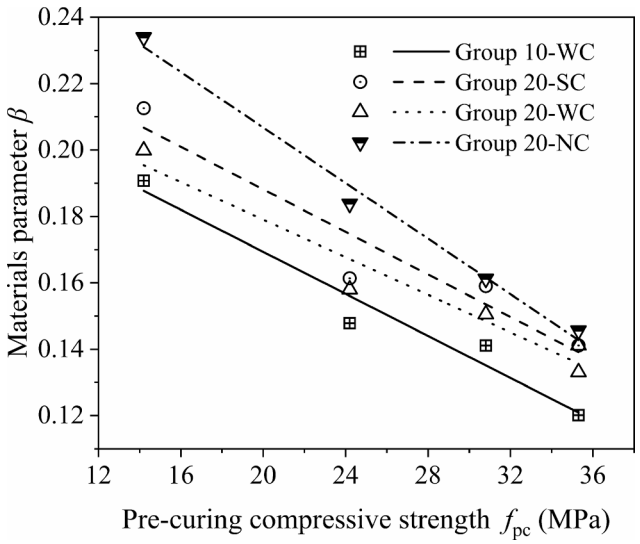


**Fig. 13.** Relationship between material parameter $\beta$ in the Yu model and pre-curing compressive strength of the damaged concrete specimens.

**Table 7**
Fitting equations for material parameter $\beta$ in the Yu model with pre-curing compressive strength $f_{pc}$.

| Groups | $\beta$ | $R^2$ |
|---|---|---|
| 10-WC | $\beta = 0.2327 - 0.00317 f_{pc}$ | 0.9570 |
| 20-SC | $\beta = 0.2522 - 0.00320 f_{pc}$ | 0.9131 |
| 20-WC | $\beta = 0.2356 - 0.00283 f_{pc}$ | 0.9466 |
| 20-NC | $\beta = 0.2904 - 0.00418 f_{pc}$ | 0.9897 |

models, the Pei model and the Yu model, were obtained, as shown in Table 4 and Table 5. The fitting curves for the two types of models are shown in Fig. 10 and Fig. 11. In general, the coefficients of determination using the Pei model were higher than those for the Yu model, which indicates that the Pei model can better characterize the development of RDME in the damaged concrete specimens compared with the Yu model.

Fig. 12 shows the relationship between the material parameters for the Pei model, $\beta_1$ and $\beta_2$, and the pre-curing strengths of the damaged concrete specimens in four test conditions; the fitting equations and coefficients of determination of $\beta_1$ and $\beta_2$ are shown in Table 6. It can be observed that $\log(-\beta_1)$ and $\log(\beta_2)$ were linearly positively correlated and linearly negatively correlated with the pre-curing strengths ($f_{pc}$) of the damaged concrete specimens in four test conditions, respectively. The coefficients of determination were all greater than 0.9000. Similarly, the relationship between the material parameter $\beta$ for the Yu model and the pre-curing strengths is shown in Fig. 13; the fitting equations and coefficients of determination of $\beta$ are shown in Table 7. $\beta$ was linearly negatively correlated with the pre-curing strengths; the fitting effect of each group was perfect.

### 3.2.3. *Freeze-thaw damage model of the damaged concrete subjected to E-FTCs*

Substituting the fitting equations for the material parameters in the Pei model (as shown in Table 6) into Eq. (4), the freeze–thaw damage model suitable for damaged concrete specimens with different pre-curing strengths based on the Pei model was obtained. A similar process was followed to produce a freeze–thaw damage model based on the Yu model. In this study, it was assumed that when the pre-curing strength $f_{pc}$ reached a certain value, termed the critical pre-curing strength $f_{pc\text{-}crit}$, the RDMEs of the damaged concrete specimens for a particular curing set-up were still greater than 60% after 300 FTCs during the later-age freeze–thaw test, meaning the resistance to freeze–thaw of the specimens met the standards described in GB/T 50082–2009 [39].

Using set-up "20-SC" as an example, the freeze–thaw damage models of the damaged concrete based on Pei model and Yu model are shown below.

Based on the Pei model:

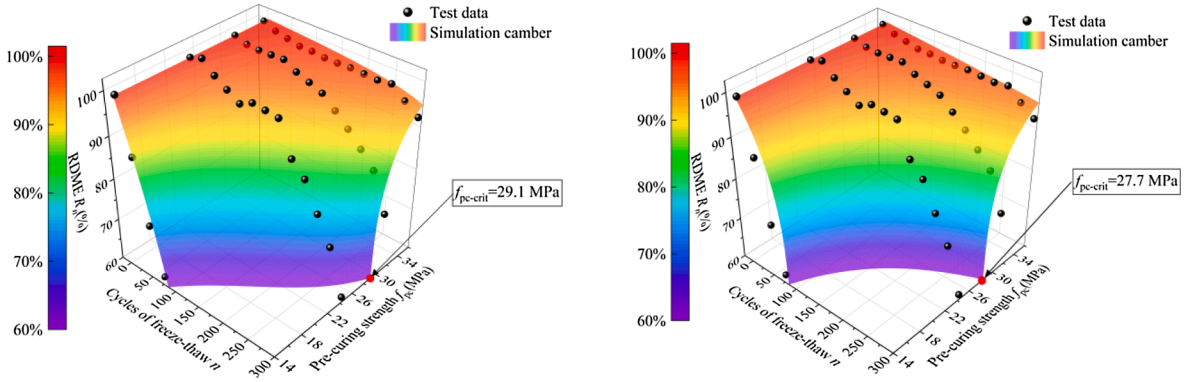


(a) the Pei model (b) the Yu model

**Fig. 14.** Prediction 3D-surface for RDME of the damaged concrete with the 20-SC set-up based on **(a)** the Pei model and **(b)** the Yu model.

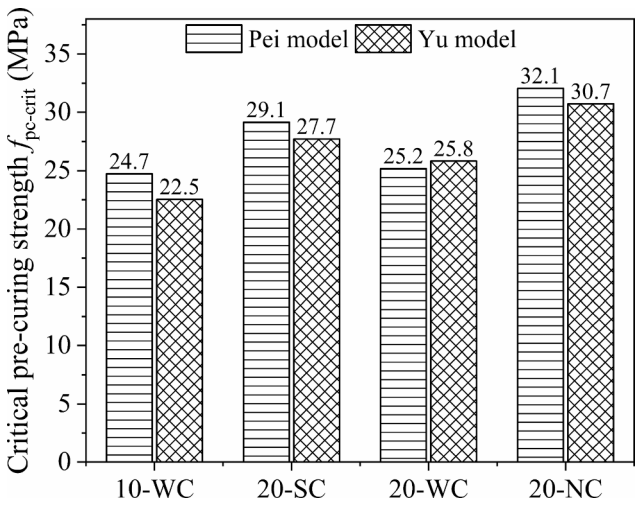


**Fig. 15.** Critical pre-curing strengths of the damaged concrete in four set-ups based on two types of models.

$$R_n = \frac{E_n}{E_0} = \left[1 - 10^{-1.32452-0.07822f_{pc}} \times n \times \left(1 + 10^{-1.05421+0.07367f_{pc}}\right)\right]^{\frac{1}{1+10^{-1.05421+0.07367f_{pc}}}} \quad (6)$$

Based on the Yu model:

$$R_n = \frac{E_n}{E_0} = \frac{0.6}{1 - (0.2522 - 0.00320f_{pc}) \times log\left(10^{\frac{0.4}{0.2522-0.00320f_{pc}}} - n\right)} \quad (7)$$

Fig. 14 (a) shows the prediction 3D-surface for RDME of the damaged concrete as a function of the pre-curing strength and the number of FTCs based on the Pei model; Fig. 14 (b) shows the prediction 3D- surface based on the Yu model. At a specified number of FTCs, with an increase in pre-curing strength, the RDME increased. Therefore, for the 20-SC set-up, the $f_{pc\text{-}crit}$ of the damaged concrete based on the Pei and Yu models are 29.1 MPa and 27.7 MPa respectively, as shown by the red dots in Fig. 14 (a) and (b).

Similarly, the critical pre-curing strengths of other three types of condition based on the Pei and Yu models are shown in Fig. 15. It can be seen that the critical pre-curing strengths of concrete based on these two models do not differ greatly. In general, among the four curing set-ups, the order of $f_{pc\text{-}crit}$ which the concrete needs to attain, from low to high, is 10-WC, 20-WC, 20-SC and 20-NC, which is consistent with the results of the resistance to freeze–thaw test described in Section 3.1.4. This means that for concrete structures expected to experience E-FTCs, it is necessary to have high pre-curing strength and appropriate subsequent curing conditions to ensure the damaged concrete can achieve acceptable freeze–thaw resistance at later-age.

## 4. Conclusions

In this study, later-age freeze–thaw resistance of damaged concrete suffering from early frost damage was evaluated by considering the influences of the pre-curing time and the curing conditions. The main conclusions are as follows:

(1) The later-age resistance to freeze–thaw of concrete specimens exposed to freeze–thaw cycles at early-age was worse than that of the control concrete that had no early-age frost damage. With increasing pre-curing time, the later-age resistance to freeze–thaw of damaged concrete gradually improved. However, the frost resistance of damaged concrete with a pre-curing time of 18 h was significantly lower than that of other concretes with longer pre-curing times.

(2) For the four curing set-ups used in this study, the resistance to freeze–thaw of damaged concrete decreased in the order of 10-WC, 20-WC, 20-SC and 20-NC. This indicates that the increase in the number of E-FTCs aggravated the frost damage to the early-age concrete, resulting in the poor later-age resistance to freeze–thaw. The re-curing conditions after exposure to E-FTCs also significantly influenced the freeze–thaw resistance of the damaged concrete at later-age. Subsequent water curing of damaged concrete produced the best resistance to freeze–thaw, followed by standard curing, while natural air curing at low humidity levels had the worst resistance to freeze–thaw.

(3) Based on the experimental results achieved in this study, prediction models of freeze–thaw damage suitable for damaged concrete exposed to E-FTCs were created, based on two previous freeze–thaw damage models. There were good correlations between the parameters of the damage model and the pre-curing strengths of damaged concrete. In addition, based on the proposed prediction model, the critical pre-curing strengths which can ensure that the damaged concrete has adequate frost resistance at later-age were obtained with four different set-ups. Results indicated that adequate pre-curing strength and good re-curing conditions are essential for concrete structures expected to be subject to E-FTCs.

## Declaration of Competing Interest

The authors declare that they have no known competing financial interests or personal relationships that could have appeared to influence the work reported in this paper.

## Acknowledgement

This project is financially supported by the National Natural Science Foundation of China (grant no. 51378104).

## References

[1] P.K. Mehta, Durability of concrete-fifty years of progress, in: Proceedings of the 2nd international conference, Montreal, Canada, SP 126-1, 1991, pp. 1–31.
[2] S. Zhang, B. Zhao, Research on the performance of concrete materials under the condition of freeze-thaw cycles, Eur. J. Environ. Civ. Eng. 17 (9) (2013) 860–871, https://doi.org/10.1080/19648189.2013.826601.
[3] Z.F. Yang, W.J. Weiss, J. Olek, Water transport in concrete damaged by tensile loading and freeze-thaw cycling, J. Mater. Civil. Eng. 18 (3) (2006) 424–434, https://doi.org/10.1061/(ASCE)0899-1561(2006)18:3(424).
[4] Y. Li, R.J. Wang, Y. Zhao, Effect of coupled deterioration by freeze-thaw cycle and carbonation on concrete produced with coarse recycled concrete aggregates, J. Ceram. Soc. Jpn. 125 (1) (2017) 36–45, https://doi.org/10.2109/jcersj2.16183.
[5] T.C. Powers, A working hypothesis for further studies of frost resistance, J. Am. Concr. Inst. 16 (1945) 245–272.
[6] T.C. Powers, R.A. Helmuth, Theory of volume change in hardened Portland cement pastes during freezing, in: Proceedings of Highway Research Board, Bulletin no. 33, Portland Cement Association, vol. 32, 1953, pp. 286–297.
[7] G. Fagerlund, Influence of environmental factors on the frost resistance of concrete: a contribution to the BRITE/EURAM project BREU-CT92-0591 "The Residual Service Life of Concrete Structures", Report TVBM–3059, Lund University, Lund, 1994, pp. 2. https://lup.lub.lu.se/record/1291975.
[8] G. Fagerlund, Predicting the service life of concrete exposed to frost action through a modelling of the water absorption process in the air-pore system, Report TVBM–7085, Lund University, Lund (1994) 1–5. https://lup.lub.lu.se/record/1273978.
[9] G. Fagerlund, Frost destruction of concrete-a study of the validity of different mechanisms, Nordic. Concr. Res. 58 (1) (2018) 35–54, https://doi.org/10.2478/ncr-2018-0003.
[10] G. Fagerlund, Service life with regard to frost attack-A probabilistic approach, in: M.A. Lacasse, D.J. Vainer (Eds.), Durability of Building Materials and Components 8, Institute for Research in Construction, Ottawa ON, K1A 0R6, Canada, 1999, pp. 1268–1279.
[11] M. Nili, A. Azarioon, S.M. Hosseinian, Novel internal-deterioration model of concrete exposed to freeze-thaw cycles, J. Mater. Civ. Eng. 29 (9) (2017) 04017132, https://doi.org/10.1061/(ASCE)MT.1943-5533.0001978.

[12] J. Tian, X.W. Wu, Y. Zheng, S.W. Hu, W. Ren, Y.F. Du, W.W. Wang, C. Sun, J. Ma, Y.X. Ye, Investigation of damage behaviors of ECC-to-concrete interface and damage prediction model under salt freeze-thaw cycles, Constr. Build. Mater. 226 (2019) 238–249, https://doi.org/10.1016/j.conbuildmat.2019.07.237.
[13] H. Cai, "Prediction model of concrete freeze-thaw durability", Ph.D. dissertation, Tsinghua Univ., Beijing, China, 1998 (in Chinese).
[14] K. Aas-Jakobsen, Fatigue of Concrete Beams and Columns. Bulletin No. 70–1. Division of Concrete Structure, Norwegian Institute of Technology, Trondheim, 1970.
[15] H.F. Yu, H.X. Ma, K. Yan, An equation for determining freeze-thaw fatigue damage in concrete and a model for predicting the service life, Constr. Build. Mater. 137 (2017) 104–116, https://doi.org/10.1016/j.conbuildmat.2017.01.042.
[16] J. Tian, W.W. Wang, Y.F. Du, Damage behaviors of self-compacting concrete and prediction model under coupling effect of salt freeze-thaw and flexural load, Constr. Build. Mater. 119 (2016) 241–250, https://doi.org/10.1016/j.conbuildmat.2016.05.073.
[17] Z. Li, L.L. Liu, S.H. Yan, M.K. Zhang, J.J. Xia, Y.L. Xie, Effect of freeze-thaw cycles on mechanical and porosity properties of recycled construction waste mixtures, Constr. Build. Mater. 210 (2019) 347–363, https://doi.org/10.1016/j.conbuildmat.2019.03.184.
[18] M. Hang, L. Cui, J. Wu, Z. Sun, Freezing-thawing damage characteristics and calculation models of aerated concrete, J. Build. Eng. 28 (2020) 101072, https://doi.org/10.1016/j.jobe.2019.101072.
[19] B. Wang, J. Pan, R. Fang, Q. Wang, Damage model of concrete subjected to coupling chemical attacks and freeze-thaw cycles in saline soil area, Constr. Build. Mater. 242 (2020) 118205, https://doi.org/10.1016/j.conbuildmat.2020.118205.
[20] Y. Fu, L. Cai, W.u. Yonggen, Freeze-thaw cycle test and damage mechanics models of alkali-activated slag concrete, Constr. Build. Mater. 25 (7) (2011) 3144–3148, https://doi.org/10.1016/j.conbuildmat.2010.12.006.
[21] H.G. Zhu, S. Yang, W.J. Li, Z.H. Li, J.C. Fan, Z.Y. Shen, Study of mechanical properties and durability of alkali-activated coal gangue-slag concrete, Mater. 13 (23) (2020) 5576, https://doi.org/10.3390/ma13235576.
[22] Y. Wei, Z. Wu, X. Yao, X. Gao, Quantifying effect of later curing on pores of paste subject to early-age freeze-thaw cycles by different techniques, J. Mater. Civ. Eng. 31 (8) (2019) 04019153, https://doi.org/10.1061/(ASCE)MT.1943-5533.0002801.
[23] S. Bai, X. Guan, G. Li, Effect of the early-age frost damage and nano-$SiO_2$ modification on the properties of Portland cement paste, Constr. Build. Mater. 262 (2020) 120098, https://doi.org/10.1016/j.conbuildmat.2020.120098.
[24] S.T. Yi, S.W. Pae, J.K. Kim, Minimum curing time prediction of early-age concrete to prevent frost damage, Constr. Build. Mater. 25 (3) (2011) 1439–1449, https://doi.org/10.1016/j.conbuildmat.2010.09.021.
[25] G. Huang, D. Pudasainee, R. Gupta, W.V. Liu, The performance of calcium sulfoaluminate cement for preventing early-age frost damage, Constr. Build. Mater. 254 (2020) 119322, https://doi.org/10.1016/j.conbuildmat.2020.119322.
[26] G. Zhang, H.Y. Yu, H.M. Li, Y.Z. Yang, Experimental study of deformation of early age concrete suffering from frost damage, Constr. Build. Mater. 215 (2019) 410–421, https://doi.org/10.1016/j.conbuildmat.2019.04.187.
[27] R. Polat, The effect of antifreeze additives on fresh concrete subjected to freezing and thawing cycles, Cold Reg. Sci. Technol. 127 (2016) 10–17, https://doi.org/10.1016/j.coldregions.2016.04.008.
[28] H. Choi, W. Zhang, Y. Hama, Method for determining early-age frost damage of concrete by using air-permeability index and influence of early-age frost damage on concrete durability, Constr. Build. Mater. 153 (2017) 630–639, https://doi.org/10.1016/j.conbuildmat.2017.07.140.
[29] X.P. Hu, G. Peng, D.T. Niu, N. Zhao, Damage study on service performance of early-age frozen concrete, Constr. Build. Mater. 210 (2019) 22–31, https://doi.org/10.1016/j.conbuildmat.2019.03.199.
[30] Y. Sang, Y. Yang, Assessing the freezing process of early age concrete by resistivity method, Constr. Build. Mater. 238 (2020) 117689, https://doi.org/10.1016/j.conbuildmat.2019.117689.
[31] W. Kong, Y.a. Wei, Y. Wang, A. Sha, Development of micro and macro fracture properties of cementitious materials exposed to freeze-thaw environment at early ages, Constr. Build. Mater. 271 (2021) 121502, https://doi.org/10.1016/j.conbuildmat.2020.121502.
[32] K.T. Koh, G.S. Ryu, K.H. Ahn, C.J. Park, J.H. Lee, Evaluation on the compressive strength of concrete incorporating high volume blast-furnace slag subjected to initial frost damage, Appl. Mech. Mater. 121–126 (2011) 2440–2444, https://doi.org/10.4028/www.scientific.net/AMM.121-126.2440.
[33] ACI 306R-16, Guide to cold weather concreting, American Concrete Institute, 488 Farmington, Hills, Michigan, USA, 2016.
[34] K.T. Koh, C.J. Park, G.S. Ryu, J.J. Park, D.G. Kim, J.H. Lee, An experimental investigation on minimum compressive strength of early age concrete to prevent frost damage for nuclear power plant structures in cold climates, Nucl. Eng. Technol. 45 (3) (2013) 393–400, https://doi.org/10.5516/NET.09.2012.046.
[35] JGJ 55-2011, Specification for mix proportion design of ordinary concrete, China Architecture and Building Press, 2011.
[36] GB/T 50081-2019, Standard for test method of concrete physical and mechanical properties, China Architecture and Building Press, 2019.
[37] GB/T 50080-2016, Standard for test method of performance on ordinary fresh concrete, China Architecture and Building Press, 2016.
[38] GB/T 50107-2010, Standard for evaluation of concrete compressive strength, China Architecture and Building Press, 2010.
[39] GB/T 50082-2009, Standard for test methods of long-term performance and durability of ordinary concrete, China Architecture and Building Press, 2009.
[40] ASTM C597-16, Standard test method for pulse velocity through concrete, ASTM International, West Conshohocken, PA, 2016.
[41] GB/T 50476-2019, Standard for design of concrete structure durability. China Architecture and Building Press, 2019.
[42] P. Li, X. Gao, K. Wang, V.W.Y. Tam, W. Li, Hydration mechanism and early frost resistance of calcium sulfoaluminate cement concrete, Constr. Build. Mater. 239 (2020) 117862, https://doi.org/10.1016/j.conbuildmat.2019.117862.
[43] Y.M. Tu, D.Y. Liu, L. Yuan, T.F. Wang, Early hydration process and kinetics of concrete based on resistivity measurement, J. Adv. Concr. Technol. 19 (3) (2021) 196–206, https://doi.org/10.3151/jact.19.196.
[44] X.S. Wei, L.Z. Xiao, Electrical resistivity monitoring and characterisation of early age concrete, Mag. Concr. Res. 65 (10) (2013) 600–607, https://doi.org/10.1680/macr.12.00127.
[45] L. Cui, J.H. Cahyadi, Permeability and pore structure of OPC paste, Cem. Concr. Res. 31 (2) (2001) 277–282, https://doi.org/10.1016/S0008-8846(00)00474-9.
[46] G. Sant, F. Rajabipour, P. Fishman, P. Lura, W.J. Weiss, Electrical conductivity measurements in cement paste at early ages: a discussion of the contribution of pore solution conductivity, volume, and connectivity to the overall electrical response, in: International RILEM workshop on Advanced Testing of Fresh Cementitious Materials, Stuttgart, Germany, 2006, pp. 213–222.
[47] Y.a. Wei, W. Guo, Z. Wu, X. Gao, Computed permeability for cement paste subject to freeze-thaw cycles at early ages, Constr. Build. Mater. 244 (2020) 118298, https://doi.org/10.1016/j.conbuildmat.2020.118298.
[48] D. Kwak, K. Kokubu, K. Uji, A. Ueno, Evaluation of concrete pore structure due to curing conditions, in: Y.S. Yuan, S.P. Shah, H.L. Lu (Eds.), International Conference on Advances in Concrete and Structures, Xuzhou, 2003, pp. 145–153.
[49] K.T. Koh, G.S. Ryu, J.H. Lee, Effect of curing method on the strength development and freezing-thawing durability of the concrete incorporating high volume blast-furnace slag subjected to initial frost damage, Adv. Mater. Res. 602–604 (2013) 962–967, https://doi.org/10.4028/www.scientific.net/AMR.602-604.962.
[50] S.Q. Zhang, M.H. Zhang, Hydration of cement and pore structure of concrete cured in tropical environment, Cem. Concr. Res. 36 (10) (2006) 1947–1953, https://doi.org/10.1016/j.cemconres.2004.11.006.
[51] R.M. Espinosa, L. Franke, Influence of the age and drying process on pore structure and sorption isotherms of hardened cement paste, Cem. Concr. Res. 36 (10) (2006) 1969–1984, https://doi.org/10.1016/j.cemconres.2006.06.010.
[52] Z.M. He, G.C. Long, Y.J. Xie, Influence of subsequent curing on water sorptivity and pore structure of steam-cured concrete, J. Cent. South Univ. 19 (4) (2012) 1155–1162, https://doi.org/10.1007/s11771-012-1122-2.
[53] X. Zhang, H. Zhao, Characterization of moisture diffusion in cured concrete slabs at early ages, Adv. Mater. Sci. Eng. 2015 (2015) 1–10, https://doi.org/10.1155/2015/154394.
[54] N.X. Quy, J. Kim, Y. Hama, Effect of 10-year outdoor exposure and curing conditions on the pore structure characteristics of hardened cement mortar, J. Adv. Concr. Technol. 16 (9) (2018) 461–475, https://doi.org/10.3151/jact.16.461.
[55] Y. Wang, M.Z. An, Z.R. Yu, S. Han, W.Y. Ji, Durability of reactive powder concrete under chloride-salt freeze–thaw cycling, Mater. Struct. 50 (1) (2017) 18, https://doi.org/10.1617/s11527-016-0878-5.
[56] R.D. Zhao, Y. Yuan, Z.Q. Cheng, T. Wen, J. Li, F.H. Li, Z.J. Ma, Freeze-thaw resistance of Class F fly ash-based geopolymer concrete, Constr. Build. Mater. 222 (2019) 474–483, https://doi.org/10.1016/j.conbuildmat.2019.06.166.
[57] W. Dong, X.D. Shen, H.J. Xue, J. He, Y. Liu, Research on the freeze-thaw cyclic test and damage model of Aeolian sand lightweight aggregate concrete, Constr. Build. Mater. 123 (2016) 792–799, https://doi.org/10.1016/j.conbuildmat.2016.07.052.
[58] W.Q. Pei, Model analysis of freeze-thaw damage deterioration of concrete based on fatigue damage theory, Railw. Constr. Technol. 5 (2014) 51–54 (in Chinese).
[59] J.L. Chaboche, P.M. Lesne, A non-linear continuous fatigue damage model, Fatigue Fract. Eng. Mater. Struct. 11 (1) (1988) 1–17, https://doi.org/10.1111/j.1460-2695.1988.tb01216.x.
[60] ASTM C666M-15, Standard test method for resistance of concrete to rapid freezing and thawing, ASTM International, West Conshohocken, PA, 2015.